Low Frequency SAS: Spatial Coherence Study

Fabien Novella, Yan Pailhas, Isabelle Quidu, Gilles Le Chenadec

Volume 40 http://acousticalsociety.org/

International Conference on Underwater Acoustics

9 September 2020

ICUA 2020

Low Frequency SAS: Spatial Coherence Study

Fabien Novella
Lab-STICC, UMR CNRS 6285 ENSTA Bretagne, 29200 Brest, FRANCE; fabien.novella@ensta-bretagne.org

Yan Pailhas
CMRE, NATO Science and Technology Organization,Viale San Bartelomeo 400, 19126 La Spezia, ITALY; yan.pailhas@cmre.nato.int

Isabelle Quidu and Gilles Le Chenadec
Lab-STICC, UMR CNRS 6285 ENSTA Bretagne, 29200 Brest, FRANCE; isabelle.quidu@ensta-bretagne.fr; gilles.le_chenadec@ensta-bretagne.fr

The notion spatial coherence is used by sonar systems such as Correlation Velocity Logs (CVL) and Synthetic Aperture Sonars (SAS). It exploits correlation between acoustic signals sensed in space and time to estimate for example platform displacement. The Van Cittert Zernike (VCZ) theorem, is a classical statistical optics theorem that predicts the spatial coherence of a pressure field backscattered by a random medium. However it appears that intrinsic characteristics of Low Frequency Synthetic Aperture Sonar (LFSAS) can breach VCZ asumptions.

In this paper, the notion of spatial coherence applied to a Low Frequency SAS system (LFSAS) is investigated. In a first part, the notion of spatial coherence and the VCZ therorem is presented. Then the High Resolution LFSAS (HRLFSAS) developed by NATO CMRE and used in this work is introduced. In the same time, a simulation tool is presented. In this paper, typical coherence functions obtained on simulation are presented. That allows to point out the link between the shape of the coherence function and the length of the transmit antenna. These functions are compared to the coherence observed on LFSAS data. Differences are investigated in terms of signal to noise ratio.

Published by the Acoustical Society of America

 https://doi.org/10.1121/2.0001320

INTRODUCTION / BACKGROUND

Over the last two decades, Synthetic Aperture Sonars (SAS) have been widely developed. They are now commonly used in different applications such as mine hunting,[1] habitat mapping,[2] underwater archaeology.[3] In all these applications, the ability of SAS systems to create high resolution images of the seabed with a resolution independent of range is very appreciated. Moreover, the frequency independence has allowed SAS manufacturers to choose central frequency for other reason than resolution. Generally speaking, highest frequency systems produce images of the seabed with a 'photographic' quality but maximum range is limited by higher sound absorption. Lower frequency systems provide greater range but the low quality images may be more difficult to be interpreted. Automatic target detection and classification as well as operator detection, need an easily interpretable image.[4] Hence most of Automatic Mine Counter Measures systems work at high frequency. With the quality of images and resolution gain Automatic Target Detection (ATR) algorithms are now close to 90% detection rate.[5] However, this detection rate is still too low and the false alarm rate is too high to be used in a fully automatic MCM system. The false alarm rate is due to ambiguities between mine-like objects and natural objects that can not be resolved even with high resolution. To deal with this issue, Low Frequency SAS (LFSAS) has been presented has a powerful tool.[6] The exploitation of LFSAS data should greatly improve the performance of ATR algorithms by providing richer information on the object (ability to distinguish objects of the same external shape but of different structure / material), reducing false alarms. It should also allow to detect buried objects. Many studies have been conducted in order to image buried targets with a SAS[7,8] or with a parametric SAS.[9]

However, if SAS image can help to locate targets on a large scene, the formation of the SAS image proves to be poorly suited to the representation of the LFSAS data.[10] Indeed, penetration into the sediment makes the LF data analysis tricky since the surface information of the object and sediment can be confused with the volume information. Therefore, LFSAS image interpretation is more difficult than for HF systems. In this paper, the notion of spatial coherence is investigated. The coherence of the acoustic signals can be used to estimate the navigation of the platform with an accuracy well below the wavelength of the system.[11] It also allows, for high-frequency SAS images, the detection of stable reflectors generally symptomatic of manufactured objects.[12] Hence it appears that spatial coherence could be used for target detection. However, the notion of spatial coherence is not well approached for low frequency systems. This paper studies spatial coherence for low frequency SAS. A basic theorem in spatial coherence is the Van Cittert Zernike theorem (VCZ). After a presentation of spatial coherence and VCZ theorem, coherence function observed on LFSAS data is presented. In the same time, a simulation tool is introduced.

1. THEORY OF SPATIAL COHERENCE

A. FUNDAMENTALS OF COHERENCE AND THE VAN CITTERT ZERNIKE (VCZ) THEOREM

In sonar, spatial coherence is a measure of the similarity of backscattered echoes received by transducer elements, as a function of element separation. The Van Cittert Zernike therorem is a well know optics theorem that predicts the coherence field from the distribution of energy across an incoherent source. According to this theorem, the spatial coherence in an observation region is the scaled Fourier transform of the intensity distribution of an incoherent source.[13] The VCZ theorem was adapted to acoustic signals by Mallart and Fink.[14] In this paper, the authors show that under some assumptions, spatial coherence is proportional to the autocorrelation of the transmitter aperture function. Therefore, if the transmitter is a linear array, its aperture function is a rectangle function. Thanks to the VCZ theorem, the coherence figure can be predicted, and it will be a triangle function whose base is twice as wide as the rectangle. The assumptions required are the

following ones:

- Narrowband signals: the VCZ theorem links the covariance of two backscattered signals to the Fourier transform of the spatial distribution of the volume reflectivity of the insonified medium. This derivation implies a constant reflectivity which is only verified for narrowband signals.
- Homogeneity of the scattering medium: the observed medium must be homogeneous, isotropic and stochastic. While this assumption seems realistic for diffuse environments such as sediments, the presence of strong reflectors in manufactured objects invalidates it.
- Born approximation: when integrating the sound field over the entire insonified volume for the calculation of the total backscattered field, the interaction between the different scattering elements is neglected. This assumption is extremely problematic in the low frequency range. Indeed, the interest of a low-frequency system lies in the access to resonance phenomena which are by nature linked to the interaction of elements internal to the structure.
- Fresnel approximation: the observation of the sound field must be made at two points of space where the difference in observation angle is small. Low-frequency systems are wide-beam in nature and therefore such a formulation does not reflect the very wide antenna aperture of the studied sonar system.

Thus it appears that the characteristics the LFSAS system studied in this project breach some of the VCZ assumptions. As explained previously, spatial coherence is a crucial point for SAS micronavigation. Therefore, in order to use LFSAS as an MCM system, VCZ derivation for such a system must be studied. To do so, a simulation tool is developed and presented in the following part with some preliminary findings.

B. PRACTICAL ESTIMATION OF SPATIAL COHERENCE

Spatial coherence between two zero-mean signals s_1 and s_2 acquired at two distinct points P_1 and P_2 is usually evaluated through the mutual coherence $J(P_1, P_2)$ and the factor of coherence $\mu(P_1, P_2)$ with:

$$J(P_1, P_2) = \Gamma(P_1, P_2)_{|\tau=0} \quad \text{and,} \tag{1}$$

$$\mu(P_1, P_2) = \frac{J(P_1, P_2)}{\sqrt{(J(P_1, P_1) \cdot J(P_2, P_2))}} \tag{2}$$

where $\Gamma(P_1, P_2)_{|\tau=0}$ is the intercorrelation between signals s_1 and s_2 evaluated at 0 temporal lag. Lets consider a sonar formed by one transmitter and four receivers lying in the same plane (see figure 1). A possible coherence as function of distance between receivers is represented in figure 1 (b).

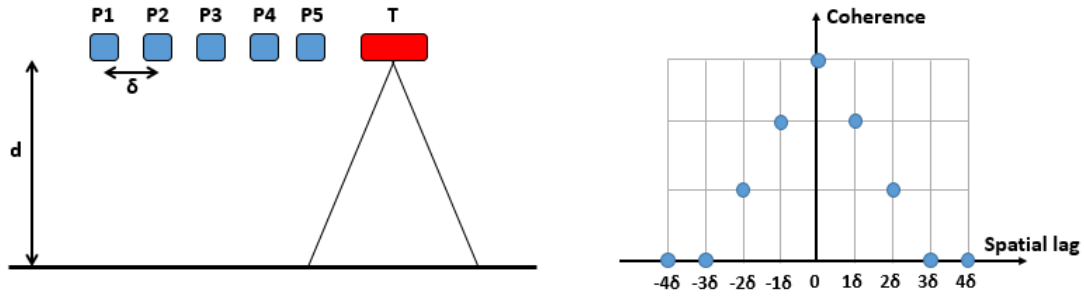

(a) **(b)**

Figure 1: (a) A one dimensional array with equally spaced hydrophones. - (b) Typical coherence function for such an array.

Practical computation of coherence function is presented here. Positions P_1 and P_2 in Eq. (1) and (2) refer the locations of receiver elements. Mutual coherence can thus be computed for each pairs of receivers by intercorrelation between signals (see Eq. (1)). Then mutual coherence is normalised by autocorellations of both signals to compute the degree of coherence (see Eq. (2)). Finally mutual coherences are grouped by element separation and averaged in order to compute the degree of coherence for a given spatial lag. Therefore, for a spatial lag d, the entire calculation is summarised by the following expression:

$$\hat{\mu}(d) = \frac{1}{N_d}\Sigma_{N_d}\frac{\left\langle s_i(t)\cdot s_j^*(t)\right\rangle_t}{\sqrt{\left\langle s_i^2(t)\right\rangle_t\cdot\left\langle s_j^2(t)\right\rangle_t}}, \tag{3}$$

where N_d is the number of receiver pairs that are separated by a distance d.

2. APPLICATION TO REAL DATA AND COMPARISON TO SIMULATION

In order to study spatial coherence of LFSAS signals a dataset from TORHEX'18 trials is used. In parallel a simulator is developed in order to evaluate influence of VCZ assumptions on coherence measurements. In the two following parts, TORHEX'18 trials and the simulation tools are presented.

A. HRLFSAS AND TORHEX'18 TRIALS

The system studied in this paper is the HRLFSAS developed by NATO CMRE. Previous publications about this system can be found.[15,16] It consists of a 2D wideband low frequency transmit antenna that insonifies a seafloor on which a 1m diameter spherical shell is lied. Echogram and SAS image are represented on figure 2.

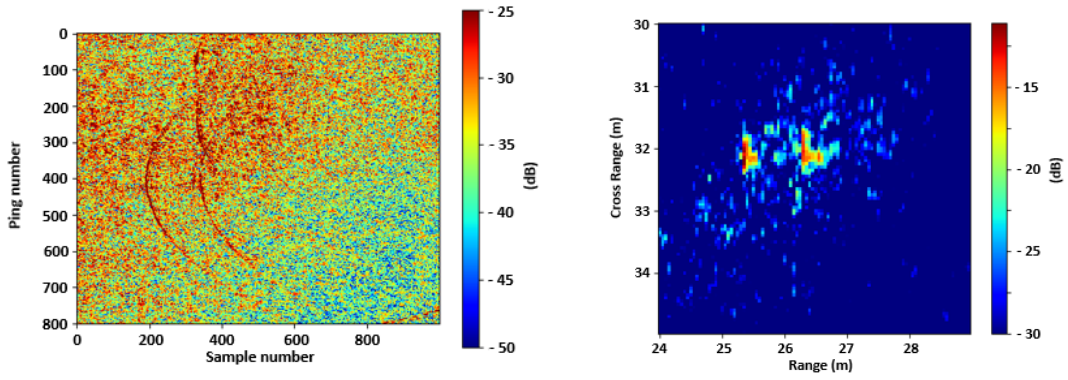

(a) **(b)**

Figure 2: (a) Echogram - (b) SAS image

From echogram (see figure 2.a), the angular aperture of the system can be deduced. From this angular aperture the length of the antenna can be computed. The angular aperture $2\theta_{-3dB} = 24°$ is read on echogram, and assuming a $15kHz$ central frequency, the emission antenna length must be around $0.21m$.

B. SIMULATION

The model used for these simulations is a classic finite scatterer model first developed for radar.[17] This model assumes a finite number of fixed scatterers P. These scatterers are located at (X_p, Y_p, Z_p). Sonar is composed by Q transmit elements located at (X_q, Y_q, Z_q) and R receivers located at (X_r, Y_r, Z_r).
Following this configuration, contribution at the r^{th} receiver coming from the p^{th} scatterer insonified by the q^{th} transmit element can be written:[17]

$$z_{rq}^{(p)} = \sqrt{\frac{E}{Q}}\zeta_p \cdot s_0\left(t - \tau_{qp} - \tau_{pr}\right) \cdot e^{-j2\pi f_c(\tau_{qp}+\tau_{pr})}, \tag{4}$$

where:

- E represents the total amount of energy emitted by the transmit antenna. Normalization by Q makes the total energy independent of the number of transmitters.
- ζ_p is the reflectivity of the p^{th} scatterer.
- s_0 is the temporal transmit signal.
- f_c is the central frequency.
- τ_{qp} and τ_{pr} are respectively time delays from q^{th} transmit element to p^{th} scatterer and from p^{th} to r^{th} receiver. They can be computed from:

$$\begin{aligned} \tau_{qp} &= \frac{1}{c}\sqrt{(X_p - X_q)^2 + (Y_p - Y_q)^2 + (Z_p - Z_q)^2} \quad \text{and,} \\ \tau_{pr} &= \frac{1}{c}\sqrt{(X_r - X_p)^2 + (Y_r - Y_p)^2 + (Z_r - Z_p)^2} \end{aligned} \tag{5}$$

Summing over the scatterers and the transmit elements, the signal received at the r^{th} receiver is:

$$\begin{aligned} z_r(t) &= \Sigma_{q=1}^{Q}\Sigma_{p=1}^{P} z_{rq}^{(p)} \\ &= \Sigma_{q=1}^{Q}\Sigma_{p=1}^{P}\zeta_p \cdot s_0\left(t - \tau_{qp} - \tau_{pr}\right) \cdot e^{-j2\pi f_c(\tau_{qp}+\tau_{pr})}. \end{aligned} \tag{6}$$

A reformulation of the previous model can be proposed in order to suit broadband sonar systems.[18] Eq. (6) becomes:

$$Z_r(f) = \Sigma_{q=1}^{Q}\Sigma_{p=1}^{P} h_{rq}^{(p)} \cdot S_0(f) \cdot e^{-j2\pi f(\tau_{qp}+\tau_{pr})}, \tag{7}$$

with :

$$h_{rq}^{(p)} = \zeta_p \cdot e^{-j2\pi f_c(\tau_{qp}+\tau_{pr})}. \tag{8}$$

C. COHERENCE STUDY

As expressed in section 1.A, the VCZ theorem predicts the size of the triangular form of the coherence function. Coherence function for HRLSAS system is represented on figure 3 (a). One can notice the triangular shape with a $20cm$ base. The dependence of the coherence function with respect to antenna length is pointed out in figure 3 (b). This figure shows coherence functions computed by simulation for different antenna lengths. Results of simulations (triangular shapes) are in accordance with VCZ predictions. However, even though it is assumed that HRLFSAS array is equivalent to a linear array of length $0.2m$, coherence functions computed on data (figure 3.a) and simulated (blue curve on figure 3.b) are quite different. The main difference is that the degree of coherence for 0 spatial lag is not 1 on real data. That point is explained in the following part.

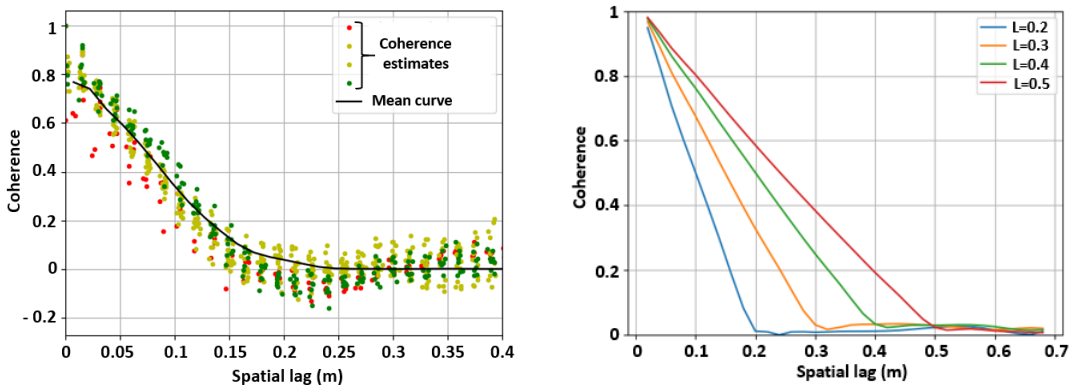

(a) **(b)**

Figure 3: (a) Coherence function estimated on TORHEX data - (b) Coherence function estimated from simulation for different transmitter lengths

D. RESULTS INTERPRETATION: INFLUENCE OF SIGNAL TO NOISE RATIO

Lets consider two signals s_1 and s_2 affected by two independent noises with a same distribution n_1 and n_2 such as:

$$\begin{aligned} s_1' &= s_1 + n_1 \quad \text{and,} \\ s_2' &= s_2 + n_2. \end{aligned} \tag{9}$$

By definition, the degree of coherence between signals s_1' and s_2' can be written by:

$$\mu_{12}' = \frac{\langle s_1' s_2' \rangle}{\sqrt{\langle s_1' s_1' \rangle \langle s_2' s_2' \rangle}}. \tag{10}$$

Because noises are independent:

$$\begin{aligned} \langle s_1' s_2' \rangle &= \langle s_1 s_2 \rangle , \\ \langle s_1' s_1' \rangle &= \langle s_1 s_1 \rangle + \langle n_1 n_1 \rangle \quad \text{and,} \\ \langle s_2' s_2' \rangle &= \langle s_2 s_2 \rangle + \langle n_2 n_2 \rangle . \end{aligned} \tag{11}$$

Injectinq (11) in (10) one gets:

$$\mu_{12}' = \frac{\langle s_1 s_2 \rangle}{\sqrt{\left(\langle s_1 s_1 \rangle + \langle n_1 n_1 \rangle\right)\left(\langle s_2 s_2 \rangle + \langle n_2 n_2 \rangle\right)}}. \tag{12}$$

Assuming that mean square level of signals s_1 and s_2 as well as mean square level of noises n_1 and n_2 are equals, we have: $\langle s_1 s_1 \rangle = \langle s_2 s_2 \rangle = \sigma_s^2$ and $\langle n_1 n_1 \rangle = \langle n_2 n_2 \rangle = \sigma_n^2$ so:

$$\begin{aligned}\mu'_{12} &= \frac{\langle s_1 s_2 \rangle}{\sqrt{\sigma_s^4 + 2\sigma_s^2\sigma_n^2 + \sigma_n^4}} \\ &= \frac{\langle s_1 s_2 \rangle}{\sigma_s^2\sqrt{1 + \frac{2}{SNR} + \left(\frac{2}{SNR}\right)^2}} \\ &= \frac{\langle s_1 s_2 \rangle}{\sigma_s^2}\left(\frac{SNR}{1+SNR}\right) \\ &= \mu_{12}\left(\frac{SNR}{1+SNR}\right),\end{aligned} \tag{13}$$

where $SNR = \frac{\sigma_s^2}{\sigma_n^2}$. Relation (13) reflects the impact of the signal-to-noise ratio on the coherence factor. This explains why, for TORHEX data and for a zero inter-sensor distance, the coherence factor is not 1.

Relation (13) can also be used in order to estimate signal to noise ratio from data. Indeed, if two signals s_1 and s_2 are expected to be fully coherent (*i.e.* $\mu_{12} = 1$) so the decrease of the value of $\mu'_{12} = 1$ is directly attributable to the signal-to-noise ratio and the two are related by the relation:

$$\rho = max\left(\mu'_{12}\right)\big|_{\mu_{12}=1} = \left(\frac{SNR}{1+SNR}\right). \tag{14}$$

From which one can deduce:

$$SNR = \frac{\rho}{1-\rho}. \tag{15}$$

On figure 3 (left), a linear extrapolation of the mean curve allows to obtain the value $\rho = 0.803$. A linear extrapolation is used because a triangular figure of coherence is expected. The estimation of SNR is thus, $SNR = 4.08$. The simulation with a $L = 0.2m$ transmit antenna length is computed again by adding independent white noises in order to obtain a $SNR = 4.08$. Results of this simulation is plotted on figure 4 (left) and it fits well with the coherence function computed on TORHEX data. On the right part, several simulations are conducted with several signal to noise ratio. A decrease on SNR leads to a decrease on peak value of coherence function.

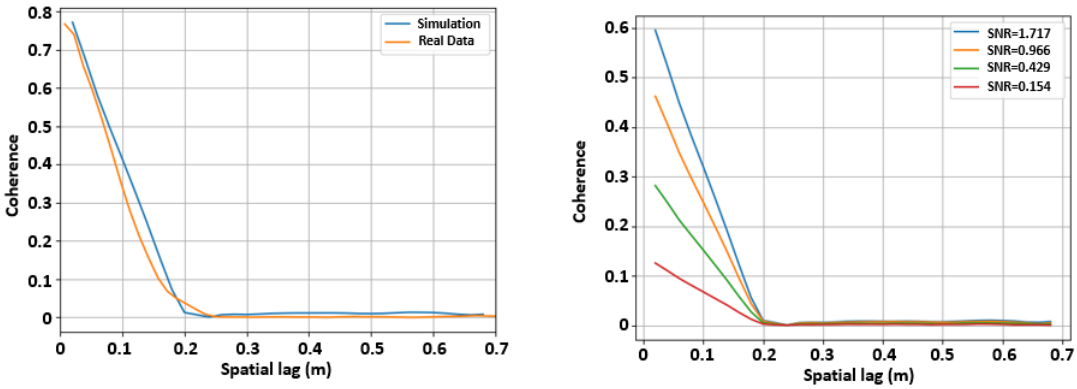

Figure 4: (a) Comparison of functions of coherence obtained on TORHEX data and by simulation using a $L = 0.2m$ transmitter length and a $SNR = 4.08$ Signal to Noise Ratio - (b) Coherence function computed from simulation for different SNR

3. CONCLUSION

In conclusion, a simulation tool has been developed in order to evaluate effects of the assumptions that LFSAS systems breach. In this paper, simulation is used to highlight the link between transmit antenna length and the shape of the figure of coherence. In accordance with the VCZ theorem, results of simulations shows that the shape of the figure of coherence is twice as wide as transmit antenna length. These results have been compared to coherence figure observe on real data. The main difference is that for a null spatial lag, real data present a degree of coherence lower than 1. The decrease is explained by the level of Signal to Noise Ratio. A relationship between degree of coherence at null spatial lag and SNR has been established. Finally, the simulation taking into account the SNR allows to notice a good agreement between real data and simulation.

ACKNOWLEDGEMENTS

This work is conducted as part of a PhD founded by AID, the French Defence Innovation Agency. We also want to thank NATO CMRE for the availability of TORHEX'18 dataset.

REFERENCES

[1] Y. Petillot, Y. Pailhas, J. Sawas, N. Valeyrie, and J. Bell. Target recognition in synthetic aperture sonar and high resolution side scan sonar using AUVs. *Proceedings of the Institute of Acoustics*, 32, 01 2010.

[2] T. Thorsnes, S. Chand, H. Brunstad, A. Lepland, and P. Lågstad. Strategy for detection and high-resolution characterization of authigenic carbonate cold seep habitats using ships and autonomous underwater vehicles on glacially influenced terrain. *Frontiers in Marine Science*, 6:708, 2019.

[3] Øyvind Ødegård, Roy E. Hansen, Hanumant Singh, and Thijs J. Maarleveld. Archaeological use of synthetic aperture sonar on deepwater wreck sites in skagerrak. *Journal of Archaeological Science*, 89:1 – 13, 2018.

[4] I. Quidu, N. Burlet, J. . Malkasse, and F. Florin. Automatic classification for MCM systems. In *Europe Oceans 2005*, volume 2, pages 844–847 Vol. 2, 2005.

[5] D. P. Williams. Underwater target classification in synthetic aperture sonar imagery using deep convolutional neural networks. In *2016 23rd International Conference on Pattern Recognition (ICPR)*, pages 2497–2502, 2016.

[6] Y. Pailhas, Y. Petillot, C. Capus, and R. Hollett. Study, design and concept of low frequency SAS. *Proceedings of the Institute of Acoustics*, 32, 01 2010.

[7] M. A. Pinto, A. Bellettini, R. Hollett, and A. Tesei. Real- and synthetic-array signal processing of buried targets. *IEEE Journal of Oceanic Engineering*, 27(3):484–494, 2002.

[8] A. Hetet, M. Amate, B. Zerr, M. Legris, R. Bellec, Jc. Sabel, and J. Groen. SAS processing results for the detection of buried objects with a ship mounted sonar. *ECUA*, 07 2004.

[9] M. Zakharia, C. Pollet, and E. Rigaud. Combined parametric synthetic and interferometric sonar for the detection of buried objects. pages 522 – 526 Vol. 1, 07 2005.

[10] J. A. Bucaro, B. H. Houston, and H. Simpson. Wide area detection and identification of underwater UXO using structural acoustic sensors. Technical report, Final Report to SERDP, Project MR-1513, 2011.

[11] A. Bellettini and M. A. Pinto. Theoretical accuracy of synthetic aperture sonar micronavigation using a displaced phase-center antenna. *IEEE Journal of Oceanic Engineering*, 27(4):780–789, 2002.

[12] Y. Pailhas, C. Capus, and K. Brown. Permanent scatterers detection using raw SAS data. *Proceedings of Meetings on Acoustics*, 17, 01 2012.

[13] J. W. Goodman. *Statistical Optics*. John Wiley and Sons, 1985.

[14] R. Mallart and M. Fink. The van cittert–zernike theorem in pulse echo measurements. *The Journal of the Acoustical Society of America*, 90(5):2718–2727, 1991.

[15] A. Xenaki and Y. Pailhas. Compressive synthetic aperture sonar imaging with distributed optimization. *The Journal of the Acoustical Society of America*, 146(3):1839–1850, 2019.

[16] Y. Pailhas, S. Fioravanti, F. Aglietti, A. Carta, A. Sapienza, and D. Galletti. Low frequency SAS 2D transmitter array calibration. In *OCEANS 2019 - Marseille*, pages 1–6, 2019.

[17] A. M. Haimovich, R. S. Blum, and L. J. Cimini. MIMO radar with widely separated antennas. *IEEE Signal Processing Magazine*, 25(1):116–129, 2008.

[18] Y. Pailhas, Y. Petillot, K. Brown, and B. Mulgrew. Spatially distributed MIMO sonar systems: Principles and capabilities. *IEEE Journal of Oceanic Engineering*, 42(3):738–751, 2017.